Growth and Characterization of Nanowires

by

Hao Ning

A Thesis Presented in Partial Fulfillment
of the Requirements for the Degree
Master of Science

Approved April 2012 by the
Graduate Supervisory Committee:

Cunzheng Ning, Chair
Hongbin Yu
Yong-Hang Zhang

ARIZONA STATE UNIVERSITY

May 2012

ABSTRACT

Nanowires (NWs) have attracted many interests due to their advance in synthesis and their unique structural, electrical and optical properties. NWs have been realized as promising candidates for future photonic platforms. In this work, erbium chloride silicate (ECS), CdS and CdSSe NWs growth by vapor-liquid-solid mechanism and their characterization were demonstrated.

In the ECS NWs part, systematic experiments were performed to investigate the relation between growth temperature and NWs structure. Scanning electron microscopy, Raman spectroscopy, X-ray diffraction and photoluminescence characterization were used to study the NWs morphology, crystal quality and optical properties. At low growth temperature, there was strong Si Raman signal observed indicating ECS NWs have Si core. At high growth temperature, the excess Si signal was disappeared and the NWs showed better crystal quality and optical properties. The growth temperature is the key parameter that will induce the transition from Si/ECS core-shell NWs structure to solid ECS NWs. With the merits of high Er concentration and long PL lifetime, ECS NWs can serve as optical gain material with emission at 1.5 μm for communications and amplifiers.

In the CdS, CdSSe NWs part, the band gap engineering of CdSSe NWs with spatial composition tuning along single NWs were demonstrated. The first step of realizing CdSSe NWs was the controlled growth of CdS NWs. It showed that overall pressure would largely affect the lengths of the CdS NWs. NWs with longer length can be obtained at higher pressure. Then, based on CdS NWs growth and by adding CdSe step by step, composition graded CdSSe alloy NWs

were successfully synthesized. The temperature control over the source vapor concentration plays the key role for the growth.

ACKNOWLEDGEMENTS

First, I would like to express my gratitude to my thesis advisor, Dr. Cunzheng Ning, who introduced me to the research field and guided me for the study in this thesis. I reaped many benefits from the group led by him, not only the knowledge, but also the hard working nature. Also, I want to thank my committee members, Dr. Hongbin Yu and Dr. Yong-Hang Zhang for their time and their insightful discussions and suggestions to my research.

Second, I am very grateful to all our group members, they helped me a lot on all aspects, in research and in daily life. It is a great experience to work with them. And the study in this thesis would not have been possible without the help from our group members. Leijun Yin, Zhicheng Liu, and Fan Fan helped me in the optical characterization of the NWs.

Finally, I would like to thank my parents for their constant support and encourage.

TABLE OF CONTENTS

Page

Chapter Page

LIST OF TABLES

Table Page

LIST OF FIGURES

Figure Page

Figure Page

Chapter 1

INTRODUCTION

1.1 Nanotechnology Background

Nanotechnology is the study of manipulation and manufacture of functional devices and systems at atomic or molecular scale. Nanotechnology offers the promise of enabling revolutionary advances in diverse areas ranging from electronics, optoelectronics, and energy to healthcare[1]. The success of realizing these potential of nanotechnology lies in the development of nanoscale materials, which have at least one critical dimension with size ranging from several to several hundred nanometers. When the size of the structure larger is than certain value, it behaves like the corresponding bulk material, which allows people to predict their properties based on the bulk counterparts. While when the size is comparable or smaller than the critical value, quantum confinement effects will be observed and the properties become size dependent. Thus, nanoscale materials exhibit unique electrical and optical properties.

There are two general approaches to producing nanoscale structures. In the top-down approach, the desired small features are patterned from larger material by using lithography techniques. This approach is relatively mature and very successful in microelectronic industry. However, resolution limit is a big problem when the size of the features goes smaller and smaller. Another problem is that it will inevitably introduce surface structure imperfection and significant crystallographic damage to the processed patterns[2], which in turn cost extra

challenges in the device design and fabrication. Improvements can be made, but there will be a near exponential increase in the cost for developing new machines and clean room environments. In the bottom-up approach, it involves creating complex assemblies with small dimension building blocks. Just like what nature has demonstrated for billions of years that complex living creatures can be produced skillfully by elementary components in a self-organization and self-construction way. It is more economical than top-down approach since there is no material waste from etching. Also, the processing procedure of bottom-up is relatively easier than top-down especially for smaller geometries.

1.2 Nanowires

Among all nanomaterial building blocks of bottom-up approach, NWs, a kind of nanostructure with the diameter on the order of nanometer and lengths on the order of micrometers, have attracted many interests due to their unique properties. Compared to other low dimensional systems, nanowire has 2 quantum confined directions but there is still one unconfined direction along which electrons and holes are free to transport. Thus, NWs exhibit significantly different electrical and optical properties compared to their bulk 3D or planar 2D counterparts. For example, they exhibit a singularity in their joint density of states, thus quantum effects would be optically observable. They also have increased surface area for electron or phonon scattering. And the two restricted transverse directions of their small diameter results in a large overlap between the electrons and holes wavefunctions, which increases the binding energy of the excitons. With many

distinctive properties, NWs have great potential to enhance the existing applications and realizing new functions.

1.3 Motivation of Erbium Chloride Silicate NWs

Microelectronics is already a mature technology that plays an important role in many aspects of our life. The desire for higher and higher capacity of carrying information for communication is driving traditional silicon microelectronics to its fundamental limits of 100 GB/s[3]. A cost effective solution is to substitute the traditional interconnects with optical interconnects. Such optical interconnects must be compatible with the current CMOS technology, but the development of silicon compatible light source and amplifier still remains challenging. This is because Si is indirect band gap material that has very short non-radiative lifetime due to strong non-radiative recombination processes. Thus it is recognized as a bad material for photonic applications.

Extensive research efforts have been made to the development of silicon compatible light sources. Among all differnt apporaches, Erbium (Er) containining materials have attracted a great deal of interest. This is because when Er incorporated into Si or silica, it can emit light at the wavelength around 1.5 μm, where optical fibers for telecommunication and computer networking have their loss minimum. Thus, it has been realized that the incorporation of optically active erbium ions into silicon will open the possibility of the developing silicon-based light sources for optical fiber communications[4].

The material in this work, single crystal erbium chloride silicate NWs[5] reported before by our group, has some superior material quality comparing with other previous erbium compound. These ECS NWs can be either Si/ECS core-shell structure or solid ECS structure. But the growth conditions and growth mechanism are not quite clear. ECS NWs growth and their properties were comprehensively and systematically investigated in chapter 3.

1.4 Motivation of CdSSe NWs

Cadmium sulfide (CdS) and Cadmium selenide (CdSe) are both the II-VI group semiconductor materials with a direct band gap of 2.42 eV and 1.73 eV respectively. Band gap is the energy difference between the bottom of conduction band and the top of the valence band. It is one of the most important semiconductor material parameters that determines the spectral information of absorption, emission and propagation for optical or optoelectronic applications. However, the bad gaps of natural semiconductors available are very limited, which hampered the capabilities in applications of these materials. In this sense, the process of controlling or altering the band gap of a material by manipulating the composition of certain semiconductor alloys, the so called band gap engineering is very important for optimizing and widening the applications of semiconductor devices. The band gap of the semiconductor alloy is determined by this equation:

$$E_g(AB_xC_{1-x}) = xE_g(AB) + (1-x)E_g(AC) + bx(1-x)$$

where b is bowing parameter, for CdSSe alloy, the value b=0.54[6]. With the advantages such as free of lattice mismatch, semiconductor alloy NWs will provide a new approach for achieving multifunctional devices compared to 2D counterparts.

Also, it is very vital to systematically find out experimental conditions under which the nanostructures are synthesized with high reproducibility and desired morphology in order to meet the needs of large-scale, controlled synthesis of nanostructures for their eventual applications. This is the fundamental step towards nanomanufacturing for future functional devices. The controlled growth of CdS NWs and band gap engineering along single CdSSe NWs were demonstrated in chapter 4.

Chapter 2

NANOWIRES GROWTH AND CHARACTERIZATION

2.1 Nanowires Growth

In 1964, Wagner and Ellis in Bell Telephone Laboratories demonstrated the vapor-liquid-solid (VLS) mechanism for anisotropic crystal growth. Now it is a very successful and widely used technique to synthesis NWs. Typically, the VLS method requires the use of metal catalyst of Au, or some other heavy metals such as Ag, Pt, Cu, Ni, Co, Ti. As for Au-Si system, the melting temperature of the Au:Si alloy reaches a minimum temperature of 363 ℃ when the Au:Si ratio is about 4:1, or the Au/Si eutectic point, which is much lower than the Si melting point of 1414 ℃. The catalyst is usually deposited as a layer of thin film on the substrate.

When the Si substrate with sputtered Au catalyst film was placed in the furnace at a temperature near or above the Au-Si eutectic point, Au-Si eutectic droplets start to form. Meanwhile, the source material that was being evaporated and transported to the substrate region will be absorbed by the surface of the eutectic droplets. When the eutectic droplets are supersaturated with source vapor, nucleation and elongation occurs at the liquid/solid interface, thus the NWs start to grow. The VLS mechanism of nanowire growth is illustrated by Figure 2.1.

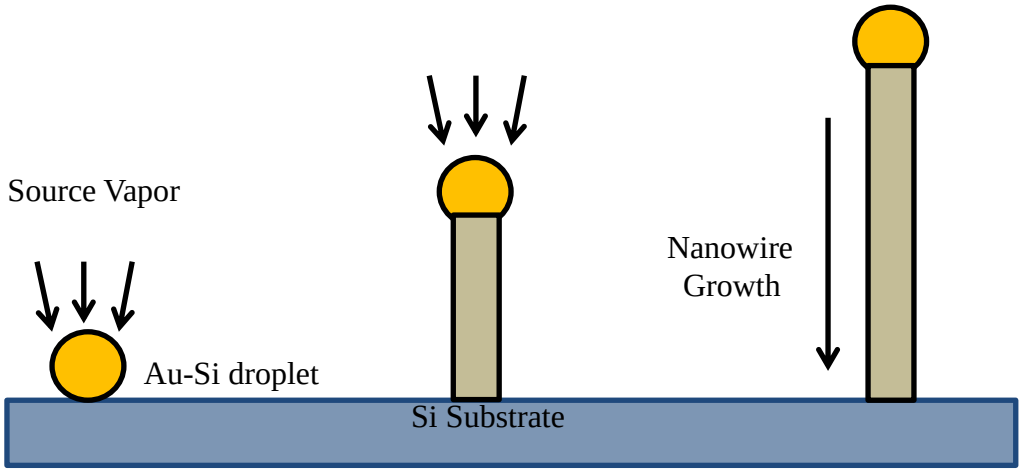

Figure 2.1 Schematic illustration of nanowire VLS mechanism growth

With the better understanding of the VLS growth mechanism, the key parameters of NWs including chemical composition, diameter, length, growth direction, and doping can be predicted and controlled. The size of the alloy droplet determines diameter of the nanowire[7]. This relates to the thermodynamic limit for the minimum radius of the droplet, given by this equation:

$$R_{\min} = \frac{2\sigma_{lv}V_l}{RT\ln(s)}$$

where R_{min} is the minimum droplet diameter, R is the wire diameter, V_l is the molar volume of the liquid droplet, σ_{lv} the liquid-vapor surface energy, and s is the degree of supersaturation of the vapor[8]. Thus, thicker catalyst film prefers wider NWs growth, while thinner film produces nanowire with smaller diameter. It has been demonstrated that using monodispersed metal nanoparticles can obtain nanowire arrays with uniform size[9]. Other parameters also affect NWs morphology, such as growth time was one of the parameter that determines the

wire length[10]. Compared to planar material growth, the free-standing NWs growth are almost free of dislocations and can accommodate large lattice mismatch more readily by lateral relaxation of strain energy.[11]

Another important feature of NWs was the controlled growth of NW axial and radial heterostructures. Nanowire axial and radial heterostructures represent compositions and/or doping tuned along or vertical to the nanowire axes. In general, the sequential alternating source vapor produces the axial heterostructures, while the direct overgrowth on the side wall of the NW by altering the conditions to favor homogeneous deposition on the surface gives radial NW heterostructures. The ability to design and synthesis diverse heterostructures distinguishes NWs from other nanomaterials such as quantum dots, opening up great opportunities for enhancing the performance and enabling new functions nanoscale photonic and electronic devices[12].

2.2 Furnace Vacuum System

The NWs studied in this thesis were synthesized in a 3-zone horizontal tube furnace. A quartz tube with an inner diameter of 1.5 inches was placed inside the furnace. The furnace system includes gas cylinder (Ar+5%H_2 or N_2), mass flow controller (MFC), flow meter, pressure controller, pump and valves as illustrated in Figure 2.2. The furnace has 3 temperature zones which can be manipulated independently, providing flexible control over the growth temperature. The flow rate of the carrier gas was controlled by mass flow controller. And there are 2 capacitance manometers that give the system pressure ranging from 1 mTorr to

atmospheric pressure with ~0.12% accuracy. And the pressure of the furnace can be controlled with a controller so that the system can maintain at any pressure in that range.

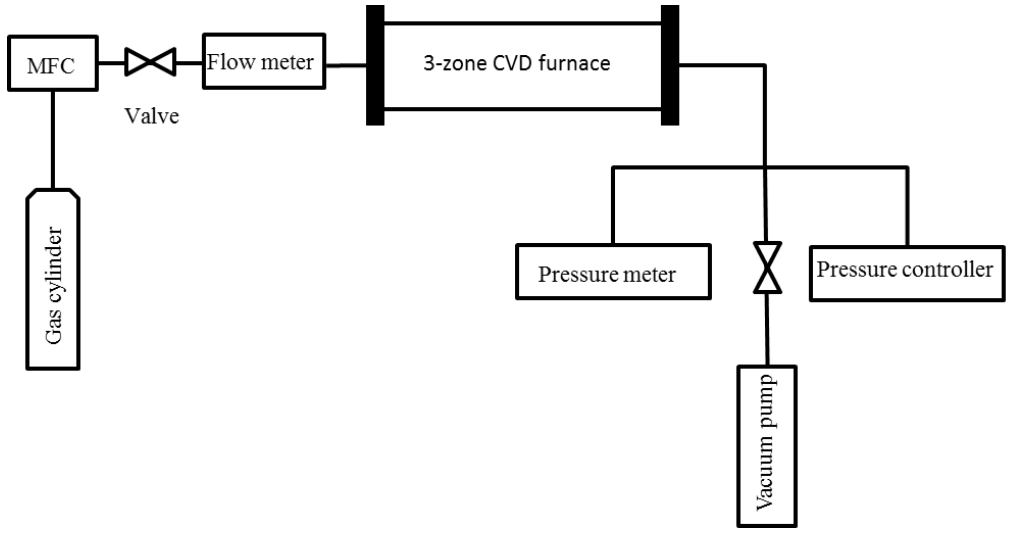

Figure 2.2 3-zone furnace vacuum system

2.3 Growth Process

The controlled growth of NWs requires good understanding of the growth process. The growth experiments require design and optimization of the different parameters including pressure, flow rate and temperature. Thus, how those parameters would affect the growth process should be studied. Typically, the growth process involves several steps as shown in Figure 2.3:

(1) Production of precursors

(2) Transport of precursors to the substrate region by the main gas flow

(3) Adsorption and diffusion of the precursors on the growth sites of the substrate surface

(4) Reactions and growth on the substrate

(5) Transport of the by-products away from the substrate.

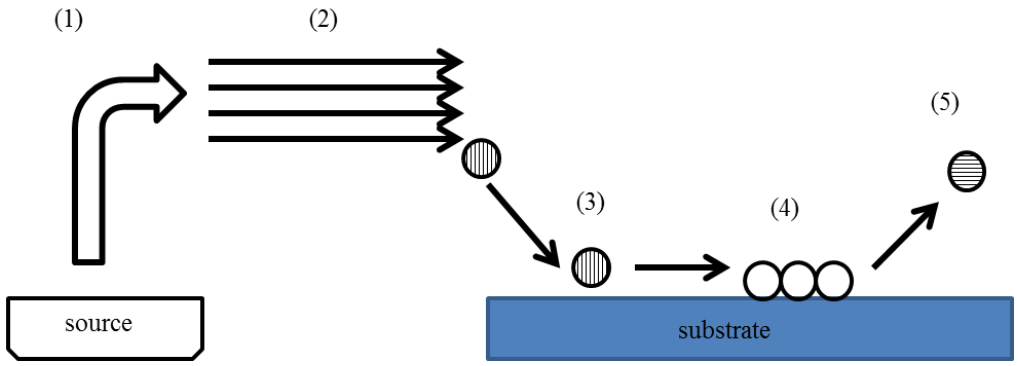

Figure 2.3 The sequence of events of the growth process

The flow can behave as either molecular flow or viscous flow and growth takes place in viscous regime. In the viscous case, low flow rates produce laminar flow which is desired, while high flow rates result in turbulent flow which should be avoided. Since the flow in the tube is laminar viscous flow, we need to consider the boundary layer issues.

The carrier gas flow velocity has a uniform value of u_0 before impinging on the leading edge of the plate. However, as flow pass through the substrate, velocity gradients will form because the gas clings to the plate because of the viscous drag from the surface. The velocity "far away" is still uniform but drops rapidly to 0 at the plate surface. The distance from the solid body at which the viscous flow velocity is 99% of the free stream velocity u_0 ($u_{(y)}$ =0.99u_0) is the so called boundary layer as shown in Figure 2.4 (a). And the thickness of the boundary layer can be expressed by the following equation[13]

$$\delta(x) = \sqrt{\frac{x}{R_e}} = \sqrt{\frac{\mu x}{\rho u_0}} \left(R_e = \sqrt{\frac{\rho u_0}{\mu}}\right)$$

where R_e=Reynolds number, a dimensionless parameter that describes the ratio of inertial forces to viscous forces, μ = viscosity, ρ= mass density, x = the distance from inlet from the flow direction. The remedy for the boundary layer problem is to tilt the susceptor at an angle, as shown in Figure 2.4 (b).

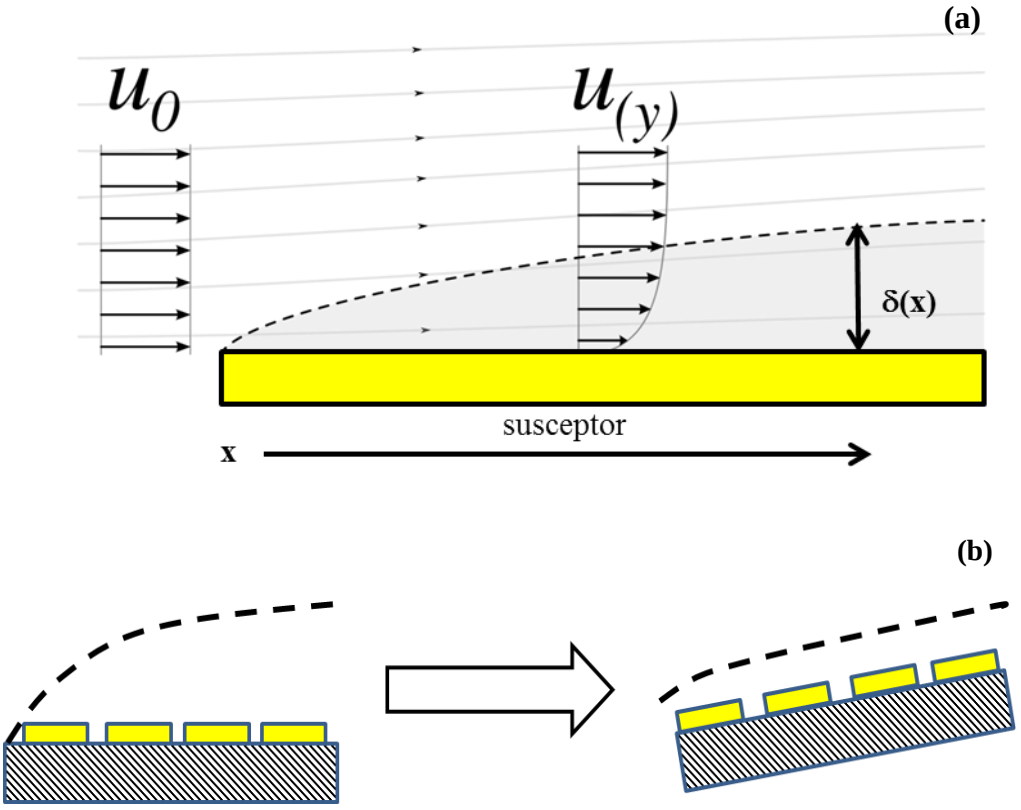

Figure 2.4 (a) Boundary Layer (b) Remedy for boundary layer

By tilting the susceptor, the uniformity of gas flow velocity profile is largely improved. As a result, source vapor is uniformly supplied to the substrate. Since the deposition uniformity and quality largely depend on the delivery of equal amount of source vapor to the entire substrate surface, more uniform deposition can be achieved in this way. Without this remedy, strong edge effect will be observed due to larger amount of source vapor supplied to the leading edge

compared to the surface at the behind. This substrate tilting strategy was used in chapter 4 for the growth of CdS, CdSSe NWs. Without tilting, there will be strong edge effect during the growth as shown in the photo in Figure 2.5 (a). With tilting, substrates have more uniform deposition as shown in Figure 2.5 (b).

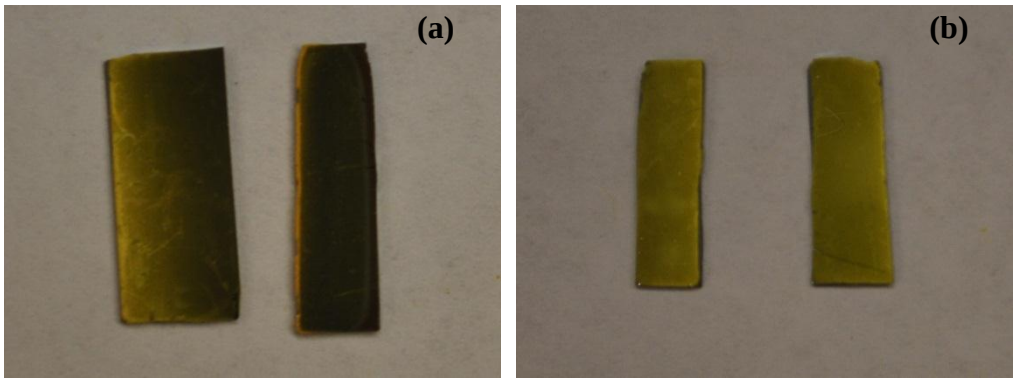

Figure 2.5 (a) Deposition with strong edge effect (b) Deposition with tilting strategy

The different experimental parameters would affect growth process in several ways. For example, the diffusibility of the gas is inversely related to its pressure, the partial pressure of the source gas vapor will largely determine the thermodynamic activity of the gas's molecules. The melting point of a substance generally increases as the pressure increases, thus pressure also affects the rate of evaporation, since evaporation happens faster if there was less exertion on the surface keeping the molecules from holding themselves. By careful optimization of all these growth parameters, the deposition can be controlled to a great degree. This is the fundamental step for the controlled NWs growth experiments.

2.4 Nanowires Characterization

2.4.1 Scanning Electron Microscopy

Scanning electron microscopy (SEM) is a type of electron microscope that use high-energy beam of electrons, which typically has energy ranging from 0.2 keV to 40 keV, for high resolution sample surface imaging. The De Broglie equation states:

$$\lambda = \frac{h}{p} = \frac{h}{mv} = \frac{h}{\sqrt{2qmV}} = \frac{1.22}{\sqrt{V}}(nm)$$

Thus, compared to optical microscope, SEM can achieve much higher resolution and larger magnification, because the wavelength of electrons ($\lambda_e = 0.0122nm = 12.2\,pm$ at V=10kV) is much shorter than visible light (390—700 nm). Magnification of a SEM can achieve in the range of about 10 to 500,000 times. In this work, the scanning electron microscopy (SEM) images were obtained by a Philips XL-30 field-emission SEM with a resolution of 3 nm.

2.4.2 X-ray Diffraction

X-rays have energies of the order of tens of kilovolts. The scattering of X-rays by periodic array of atoms can be used to identify their spatial arrangement, thus we can learn the structure of the material. The mechanism of X-ray diffraction (XRD) can be explained by considering crystals as composed of parallel planes of atoms with a spacing of d. The incident X-rays would produce Bragg peaks only if the reflected beams from the planes interfered in a

constructively way, the phase shift is a multiple of 2π . This can be expressed by Bragg's law:

$$n\lambda = 2d\sin\theta$$

where d is the spacing between the atomic planes, θ is the angle of the incident beams, n is the diffraction order, λ is the wavelength of the x-ray, as illustrated in Figure 2.6. XRD gives the atomic structure information of the material, such as quality of single crystal, composition and orientation. In this work, XRD data were collected by the PANalytical X'Pert Pro materials research X-ray diffractometer.

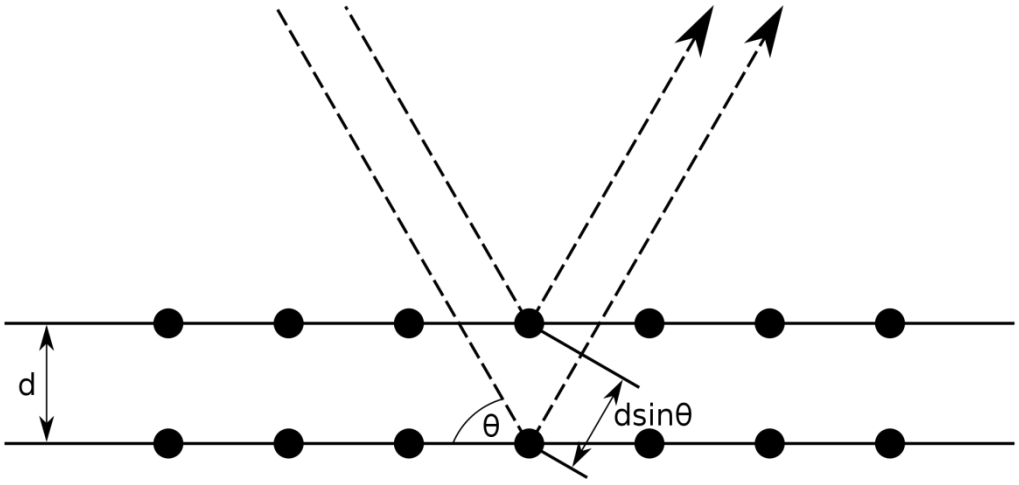

Figure 2.6 Bragg condition of X-ray diffraction in a crystal lattice

2.4.3 Photoluminescence Spectroscopy

Photoluminescence (PL) spectroscopy was a contactless, nondestructive characterization process, in which a sample absorbs photons and then re-radiates photons. The sample was excited by incident laser, which typically has energy of

$h\upsilon > Eg$, creating electron-hole pairs (ephs) that recombine and emit photons. The general PL process of direct band gap material was shown in Figure 2.7, it involves the following steps:

(1) Absorption: electron-hole (e-h) pairs are generated and excited to a non-equilibrium state by absorption of photons provided by incident light.

(2) Relaxation: the thermalization of the photo-excited e-h pairs via carrier-carrier and carrier-phonon scatterings, and relax to the lowest energy state.

(3) Recombination: the e-h pairs recombine in radiate process at the band edge.

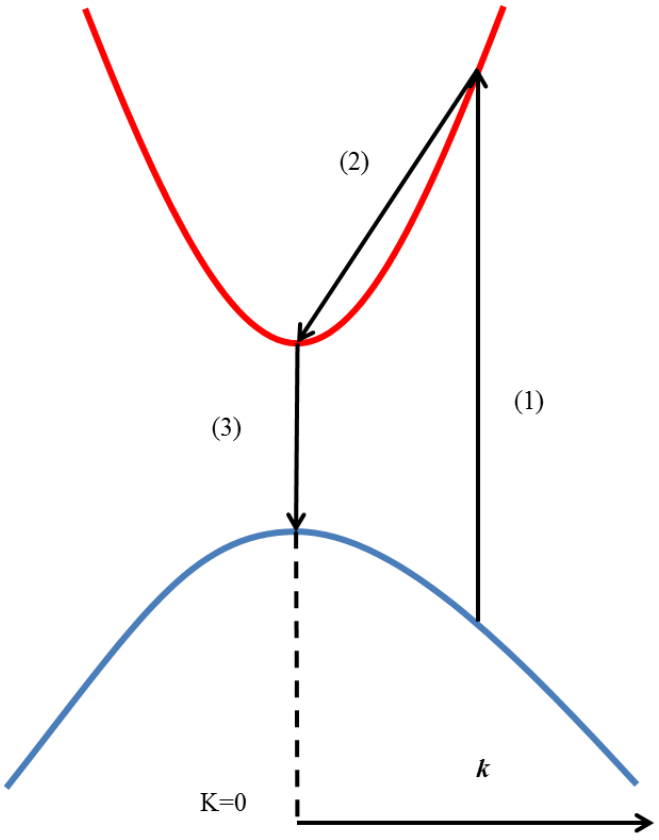

Figure 2.7 Photoluminescence process of direct band gap material

There are also non-radiated processes in which carriers recombine without emitting photo but generate phonon instead, such as Shockley-Read-Hall (SRH) process, Auger process. For SRH process, the electron in transition between bands first falls into a “trap”, the new energy state created within the band gap by an impurity or defect, then falls into an empty state in the valence band, thus completing the recombination process by energy exchange in the form of lattice vibration, or phonon. It is also called trap-assist process. For Auger process, e-h pairs will recombine in a band-to-band transition and give off the resulting energy to another electron or hole through thermal vibration. The comparisons of these processes are shown in Figure 2.8. PL gives many information of the material such as band gap, defects, and impurities. It is widely used for characterization of direct-band gap semiconductors.

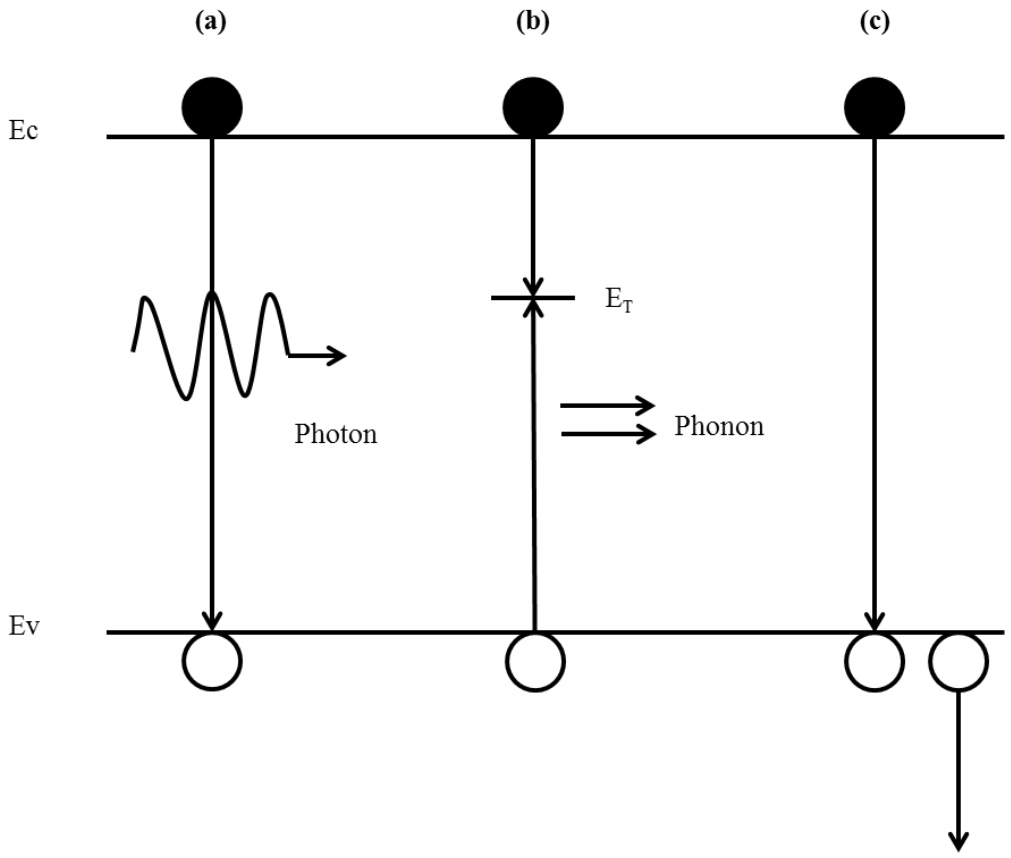

Figure 2.8 Recombination processes: (a) Raidative (b) SRH (c) Auger

2.5 Nanowires Applications

Semiconductor NWs have been successfully assembled into many electronic and photonic devices so far, such as nanowire p-n diodes[14], nanowire FETs[15], nanowire LEDs[16]. Moreover, individual NWs have the inherent nature of 1D geometry, high index of refraction (n>2) in contrast to surroundings which provide strong confinement, NWs represent a highly attractive class of material for lasing applications.

NWs lasers have some unique features compared to conventional edge emitting lasers. The facets of the NW can't be simply treated as 2 reflectors that

form a Fabry-Perot optical cavity. This is because NWs diameter is typically smaller than the lasing wavelength and thus the two facets involve diffraction loss. In this regards, for NW lasers, optical field would "spill" out of the wires due to diffraction.

In order to lase, the following condition must be fulfilled: the round-trip gain exceeds round-trip loss (threshold condition)[17]

$$\Gamma g_{th} = \alpha_w + \alpha_m$$

in which Γ was confinement factor, α_w, α_m ($\alpha_m = \frac{1}{L}\ln\frac{1}{R_1 R_2}$, L is nanowire length and R_1 and R_2 are reflection coefficient of the two facets) are waveguide loss and mirror loss respectively. Traditional edge emitting lasers have larger waveguide loss than mirror loss, but nanowire lasers have very small cavity length and small reflection coefficient[18], mirror loss dominates ($\alpha_m >> \alpha_w$) due to diffraction as discussed before. We can see that the key parameters that will determine the threshold gain are the NW length L and NW diameter D. It has been demonstrated that NWs with diameters smaller than certain critical value will never reach threshold no matter what the nanowire length is[19]. The waveguide mode spacing is given by[17]

$$\Delta\lambda = \frac{1}{L}[\frac{\lambda^2}{2}(n - \lambda\frac{dn}{d\lambda})^{-1}]$$

in which L is the cavity length and n is refractive index at certain wavelength λ. We can see that mode spacing is proportional to the inverse of cavity length 1/L.

So far, researchers have reported lasing from these nanostructure material: ZnO NW arrays (λ ~ 385 nm)[20], ZnS (λ∼337 nm) nanoribbons[21], CdS NWs (λ∼510 nm)[22],GaN ring resonator (λ∼375 nm)[23], and GaSb NWs (λ∼1550nm)[24].

Chapter 3

ERBIUM CHLORIDE SILICATE NWs

3.1 The Growth of ECS NWs

Single crystal erbium silicate (ECS) NWs in this study are grown by low pressure CVD (LPCVD) process using Vapor-Liquid-Solid (VLS) method. Silicon powder (Alfa Aesar, 99.99%) and erbium chloride ($ErCl_3$, Alfa Aesar, 99.9%, diameter ~1 mm) micro beads were used as source materials. Silicon powder was placed at the middle region of the furnace since it requires higher temperature to evaporate (Si melting point is 1414 ℃). The $ErCl_3$ source was placed at the downstream where has lower temperature. Si (100) wafer pre-sputtered with a 10 nm thickness layer of Au film was used as substrate, which was placed vertically at the behind of the $ErCl_3$ source boat. There are 2 reasons for this placement, one is $ErCl_3$ has lower evaporation temperature ($ErCl_3$ melting point was 776 ℃), and the other is $ErCl_3$ has high vapor pressure (or high volatility). In this way, $ErCl_3$ vapor can be supplied to the substrate efficiently, otherwise there will be a supply deficiency in $ErCl_3$. The substrate can't be placed horizontally for the same reason. After the furnace system was evacuated to a vacuum level of pressure below 200 mTorr by mechanical pump, a constant flow of 50 sccm Argon gas with 5% of H_2 (Standard Cubic Centimeters per Minute) was introduced into the system as the carrier gas to transport the gas phase Si and $ErCl_3$ to the substrate region. The center of the furnace was heated to temperature of 1100/1200 ℃ in around 20 minutes and then maintained for one and half hour. After the growth, the CVD

furnace was cooled down to room temperature naturally. The ECS NWs growth set-up is shown in Figure 3.1 and temperature profile of the furnace is shown in Figure 3.2. The substrate temperature can be determined by checking the position and temperature profile.

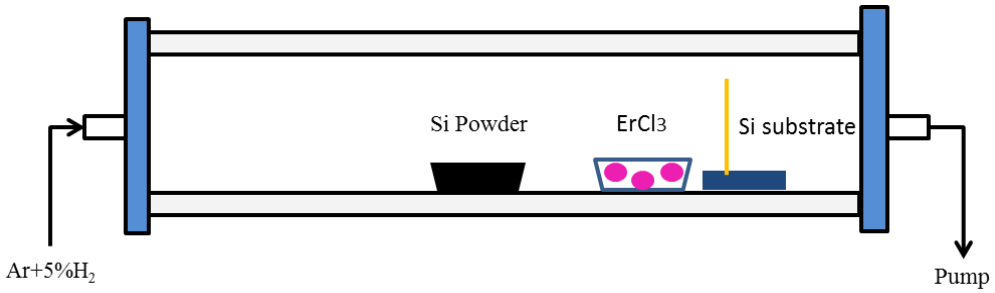

Figure 3.1 ECS NWs growth experiment set-up

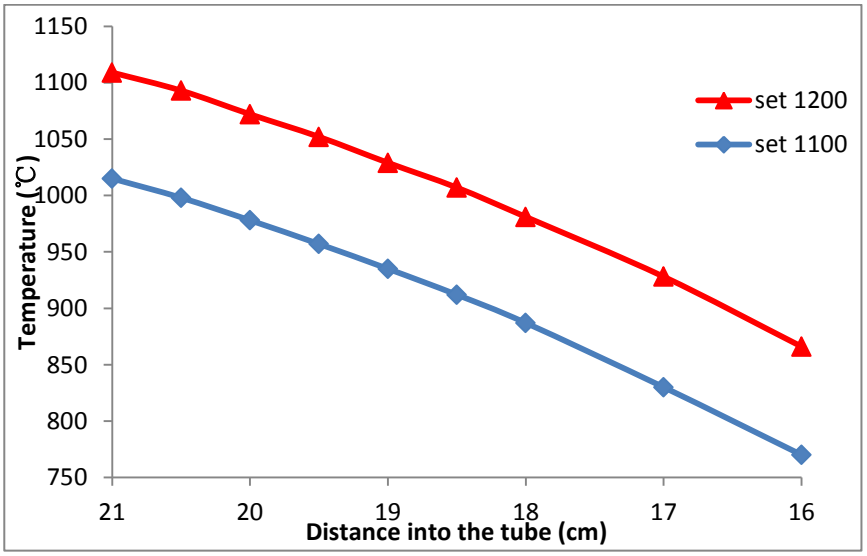

Figure 3.2 Temperature profile of the CVD furnace Blue: set temperature at 1100 ℃, Red: set temperature at 1200 ℃

In order to investigate the relationship between the NW properties and growth conditions, 2 series of experiments have been carried out. One series was performed by keeping the temperature of the center of the furnace at 1100 ℃ and

placing the substrate at different positions. The other one was setting the temperature at 1200 ℃. Thus, ECS NWs synthesized at different substrate temperature ranging from ~700 ℃ to ~1100 ℃ were obtained. The growth conditions of ECS NWs are summarized in Table 3.1.

Table 3.1Growth conditions of ECS NWs

Gas	Ar+5% H_2
Flow rate	50 sccm
Pressure	3 Torr
Source temperature	1100/1200 ℃
Substrate temperature	770-1109 ℃
Au film thickness	10 nm

3.2 Characterization of ECS NWs

To study the morphology of the NWs, scanning electron microscopy (SEM) was performed. The obtained ECS NWs typically have diameters in the range of 200-800 nm and lengths of tens of micrometers, as shown in the SEM images of the as grown samples in Figure 3.3. And the observation of the Au tips confirms the VLS growth of the NWs.

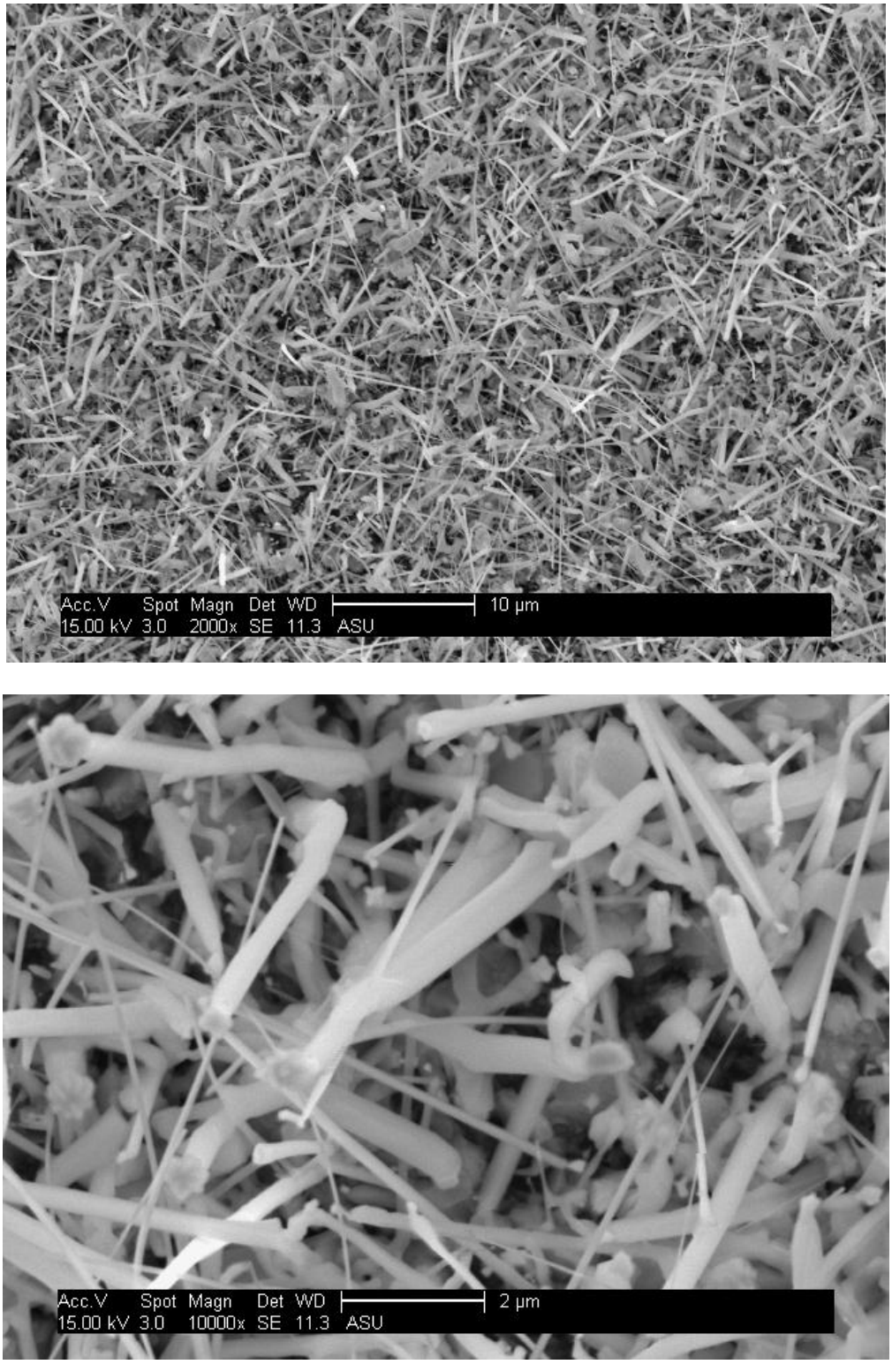

Figure 3.3 SEM images of as grown ECS NWs

Raman spectroscopy was also performed to study the ECS NWs. A 50 mW 532 nm laser was focused to the sample through an objective. At this excitation wavelength, both the Er^{3+} luminescence and Si Raman signal could be excited. Figure 3.4 (a) shows the PL/Raman spectrum of different ECS NWs samples 1, 2 and a Si wafer respectively under the same experiment conditions. A series of peaks observed from the ECS NWs 1 corresponds to the photoluminescence signal of Er^{3+} (downward transition from $^4S_{3/2}$ to $^4I_{15/2}$), which are also found on the ECS NWs sample 2 with much weaker intensity. Moreover, there is a strong peak observed at the center of the spectra for ECS NWs sample 2 while the ECS NWs sample 1 showed a double peak which comes from the PL feature of Er^{3+}. A zoomed in feature are shown in Figure 3.4 (b). It was found that the peak position of ECS NWs sample 2 was very close to the Raman signal from Si wafer. With further comparison of this peak position to Si Raman signal, it has stronger intensity, downshift and asymmetric broadening at 520 cm^{-1}, which has a good agreement with the previous reported features of Raman spectroscopy of Si NWs[25].

The most likely reason for these features is that ECS NWs 1 are solid ECS NWs which do not have excess Si Raman signals, while for ECS NWs 2 are Si/ECS core-shell NWs structure which exhibit strong Si Raman signals.

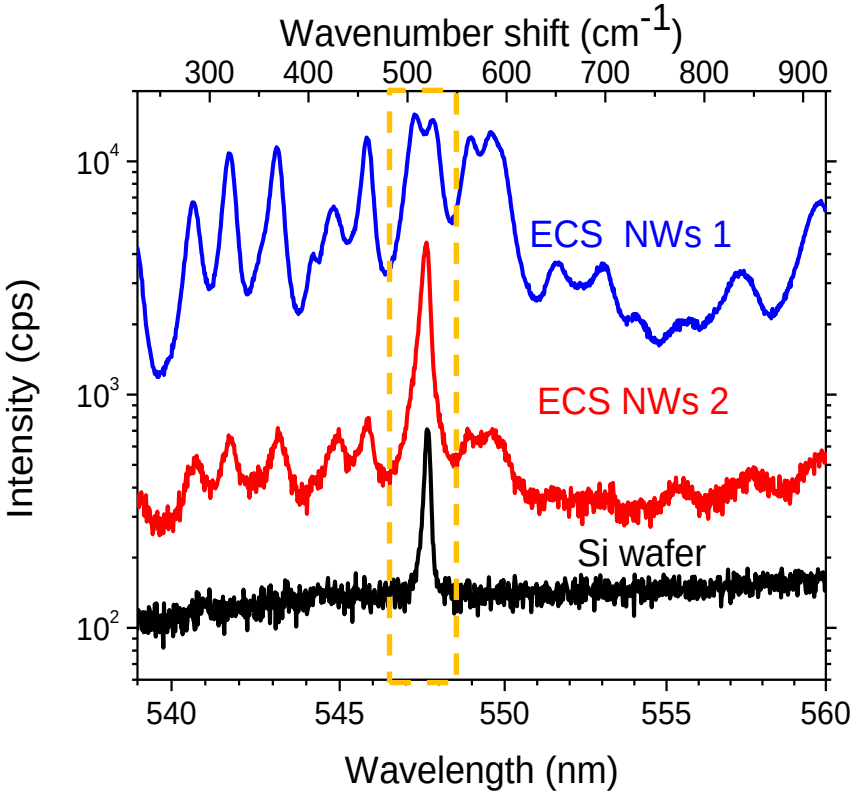
Wavenumber shift (cm-1)
300
400
500
600
700
800
900
Intensity (cps)
10^4
10^3
10^2
ECS NWs 1
ECS NWs 2
Si wafer
540
545
550
555
560
Wavelength (nm)

(a)

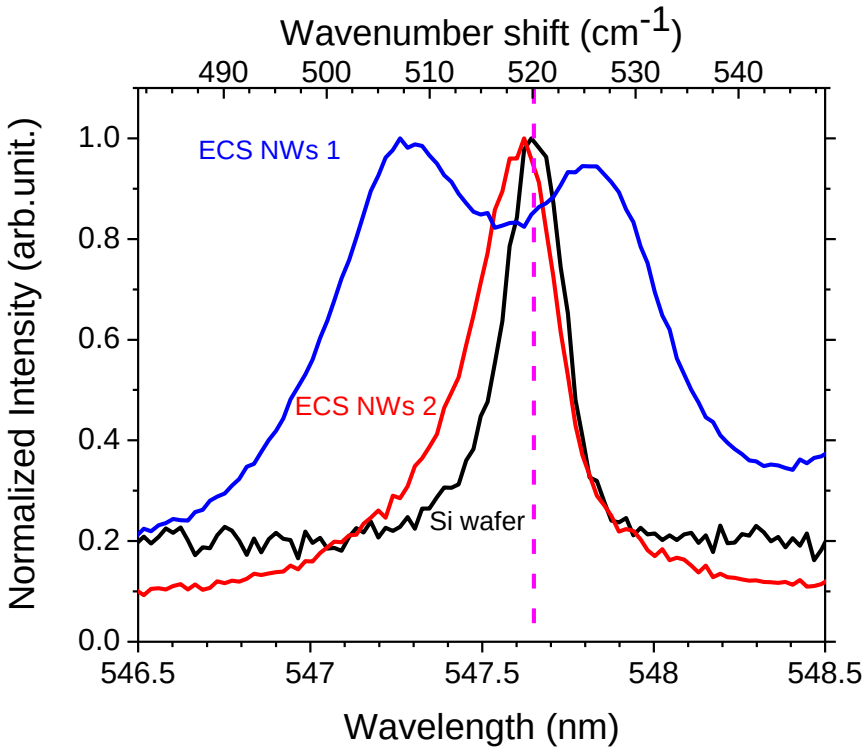
Wavenumber shift (cm-1)
490
500
510
520
530
540
Normalized Intensity (arb.unit.)
1.0
0.8
0.6
0.4
0.2
0.0
ECS NWs 1
ECS NWs 2
Si wafer
546.5
547
547.5
548
548.5
Wavelength (nm)

(b)

Figure 3.4 (a) PL / Raman comparison of different ECS NWs samples and Si wafer (b) zoomed in features

The Raman sutdy of a series of ECS samples grown at different temperature were performed. Figure 3.5 (a) shows that for ECS NWs grown at a high temperature of above 950 ℃, there is no Si signal observed and the ECS NWs exhibit very similar spectral shape. While the samples grown below 900 ℃ all showed strong Si Raman signal, which could be coming from the Si core. Thus, the samples around the transition temperature, 887 ℃, 912 ℃ and 957 ℃ were compared by the zoomed in feature shown in Figure 3.5 (b). The sample grown at 912 ℃ showed both Si Raman signal and the PL signal from Er^{3+}. Moreover, the strength of Si Raman signal for this sample was found to be weaker than the sample grown at 887 ℃ when a three-Lorentz function fitting was applied. The possible reason for such behavior is that the size of Si core of those Si/ECS core-shell NWs is shrinking and finally disappears when substrate temperature is increased. The ECS NWs have witnessed a transition from Si/ECS core-shell structure to solid ECS NWs structure.

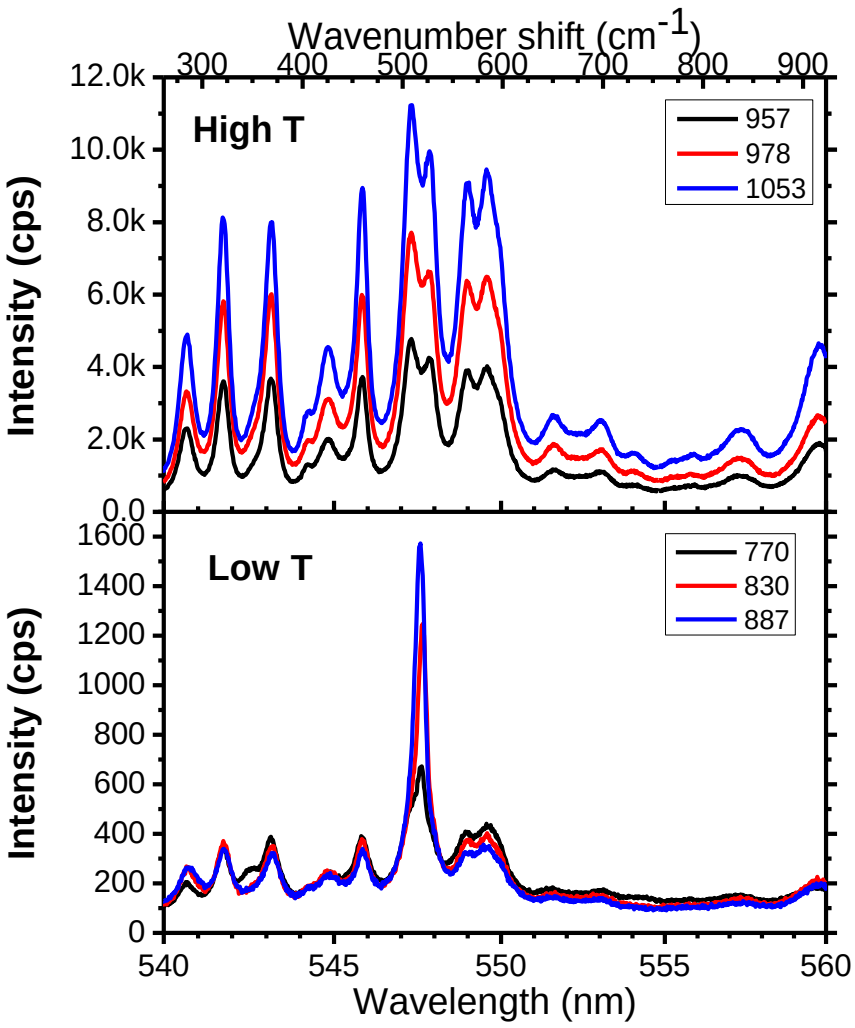
Wavenumber shift (cm-1)
300
400
500
600
700
800
900
12.0k
10.0k
8.0k
6.0k
4.0k
2.0k
0.0
High T
957
978
1053
Intensity (cps)
1600
1400
1200
1000
800
600
400
200
0
Low T
770
830
887
Intensity (cps)
540
545
550
555
560
Wavelength (nm)

(a)

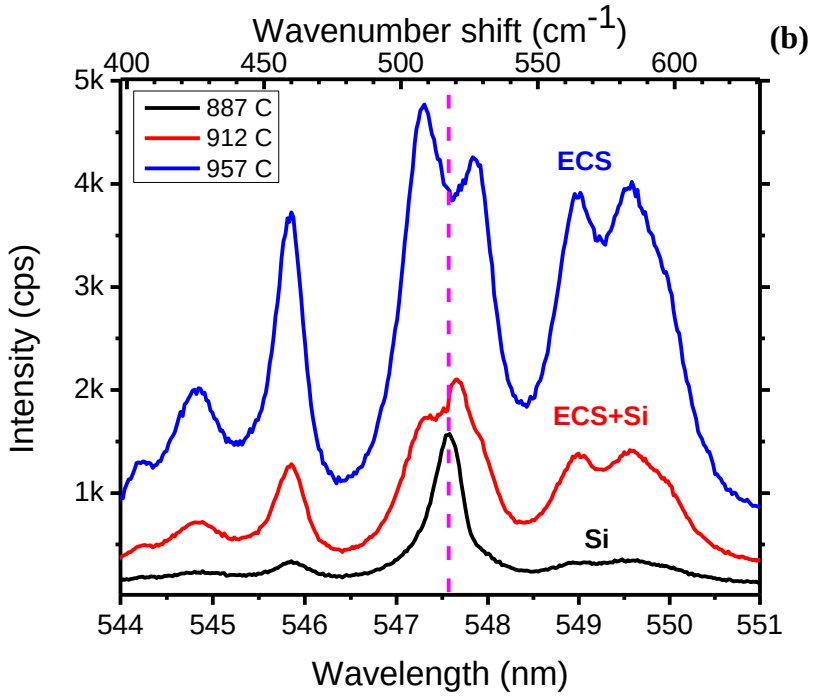

Figure 3.5 (a) PL/Raman spectra of ECS samples grown at low temperature and high temperature (b) zoom-in spectra comparison of ECS samples around transition temperature

XRD characterization was performed to further study the relation between growth temperature and ECS NWs crystal quality. From the analysis in Figure 3.6 (a), the sample grown at high temperature, the XRD peaks have a perfect match with the ECS reference peaks and there is no Si peak observed. Also, there are several Au peaks observed due to the use of Au film as catalyst. In Figure 3.6 (b), the low growth temperature case, there are both ECS peaks and Si peaks observed in the XRD pattern. To further study the crystal quality of the ECS NWs, the XRD Full width at half maximum (FWHM) of the strongest peak at 30.38 corresponding to (060) plane of ECS NWs grown at different temperature from 712 ℃ to 1072 ℃ were compared as shown in Figure 3.7. It showed a clear trend that NWs grown at

higher substrate temperature have narrower XRD FWHM compared to the samples grown at low temperature, which indicates the improvement of the ECS crystal quality when the growth temperature was increased. The sample with narrowest FWHM of 0.17 °was observed from the one grown at highest temperature. This behavior is similar to the reported feature of erbium containing thin film growth that high temperature post annealing above 1000 ℃ will improve the crystal quality[26].

(a)

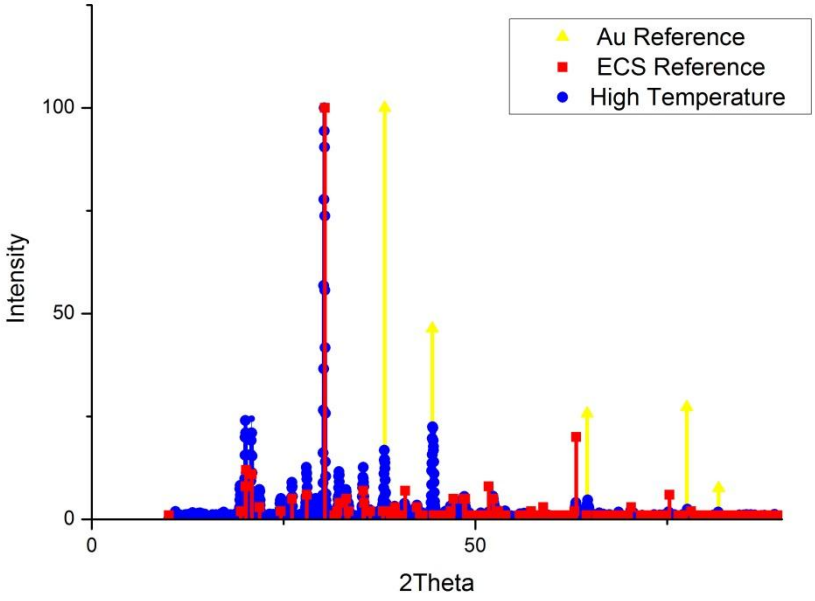

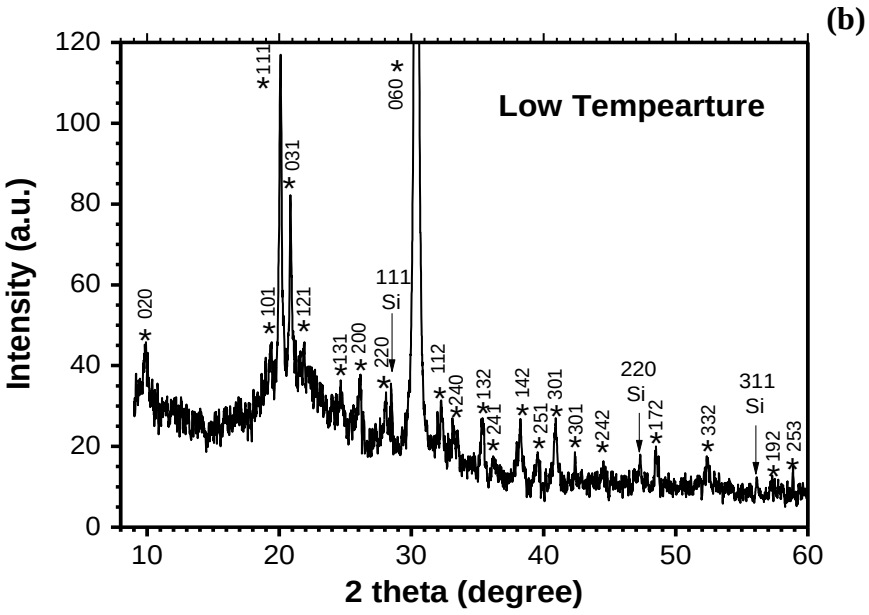

Figure 3.6 XRD analysis of ECS grown at (a) High temperature (b) Low temperature

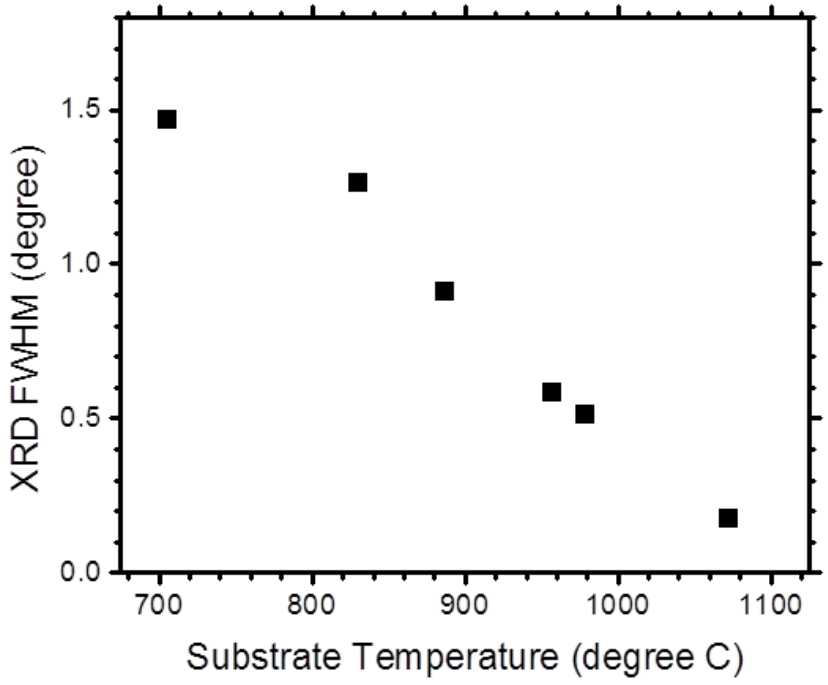

Figure 3.7 The XRD FWHM of the strongest peak at 30.38 (060) plane of ECS NWs as a function of substrate temperature

The improvement of crystal quality is further confirmed by PL decay lifetime measurement of 1.5 μm emission, a 667 nm pulse laser is used for optical excitation. The lifetime of ECS NWs samples grown at different temperatures were compared, as shown in Figure 3.8. For those ECS NWs samples grown at low temperature below 900 ℃, the lifetime is about 100 μs and there is a slightly increase as the substrate temperature is elevated. While for those samples with growth temperature above 900 ℃, there is a much faster increase in lifetime than the low temperature case. The highest lifetime of 540 μs was observed from the sample grown at highest temperature at 1072 ℃. The relation between PL lifetime and other processes is determined by following equation:

$$\frac{1}{\tau_{PL}} = \frac{1}{\tau_r} + \frac{1}{\tau_{nr}}$$

where τ_{PL} is PL lifetime, τ_r is radiative process lifetime and τ_{nr} is non-radiative process lifetime. Thus, the longer PL lifetime indicates the reduced of non-radiative recombination processes which typically caused by defects in the crystal. Below 900 ℃, the lifetime only increases with a slope of ~ 0.23 μs/ ℃, while above 900 ℃, the lifetime improvements are more dramatic with a slope of ~ 2.9 μs/ ℃. The transition temperature at around 900 ℃ agrees very well with the previous Raman results. The conclusions from all of these characterization results are the crystal quality of the ECS NWs is improved and lifetime is increased when the growth temperature is elevated.

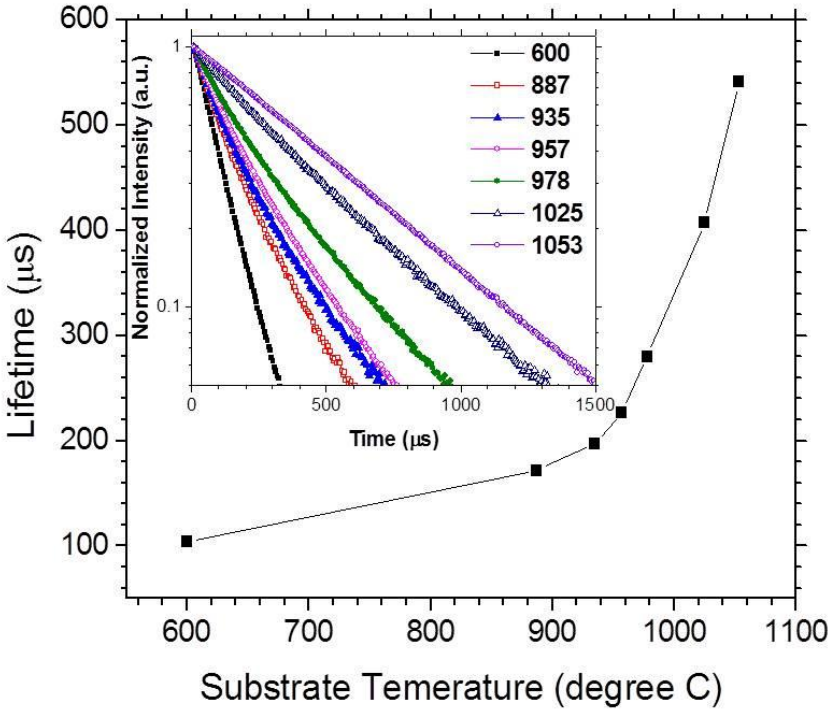

Figure 3.8 1.5 μm PL lifetime of samples grown at different temperature; Inset: PL decay curve

3.3 Growth Mechanism of ECS NWs

The minor amount of H_2O, SiO_2 and O_2 in the furnace serves as the source of oxygen for the growth of ECS NWs. The reaction can be demonstrated by the following equation:

$$ErCl_3 + Si + \text{Oxygen } (O_2, H_2O, SiO_2) \longrightarrow \text{ ECS + by-products}$$

The formation of the core-shell structure at low substrate temperature can be explained by following reasons. Er has low solubility in Si and Er has a strong surface segregation during the growth of Si[27]. The surface segregation is due to large atomic size of Er compared to Si (0.17 and 0.11 nm, respectively). But, when

the temperature is increased, the $ErCl_3$ source vapor concentration increases much faster than Si source vapor. The chemical equilibrium moves to the direction that produces more ECS according to Le Chatelier's principle, which states that when a chemical system at equilibrium experiences a change in concentration, temperature, volume, or partial pressure, then the equilibrium shifts to counteract the imposed stimulus and establishes a new equilibrium status. Thus, there is a transition in NWs morphology from core-shell structure to solid ECS structure when growth temperature is increased.

3.4 Applications of ECS NWs

The key parameters that will determine the performance of erbium based devices such as optical amplifiers and lasers are the erbium concentrations, the lifetime of the excited states and the linewidth of the emission spectrum.

Till now, there are several Si based material embedded with Er ions forms have been reported and they can be divided into two groups: Er-doped material, such as Er-doped crystalline Si[28] and Erbium doped fiber amplifier (EDFA)[29], and Er-compounds including Er_2O_3[30], Erbium Silicate (ES) in the forms of Er_2SiO_5 or Er_2SiO_7[31,26] The Er concentration in Er-doped material is limited to about 10^{20} cm^{-3} due to low solubility of Er in these materials[32]. Thus these Er-dpoed materials typically have small optical gain. While for erbium compounds, the concentration can achieve the order of 10^{22} cm^{-3}, this is because Er^{3+} ions are arranged in a periodic way so that erbium clustering problem in Er-doped material is eliminated. But those materials have short

photoluminescence (PL) lifetime, in specifically, Er_2O_3 and Er_2SiO_5 only have 5.7 and 20 μs. Thus, the threshold is high and population inverstion is hard to achieve in those materials.

For ECS NWs, the erbium concentration can achieve 1.6×10^{22} cm^3 and linewidth of only 0.8 nm, the narrowest linewidth from erbium compounds to the best of our knowledge[5]. Moreover, they have lifetime of 540 μs, the longest among all Er-materials with density above 10^{22} cm^{-3}. In this sense, ECS is capable to serve as optical gain material at the wavelength of 1.5 μm.

3.5 Conclusions

In summary, a systematic growth study on ECS NWs was performed. The characterization results confirmed that the structure and quality of ECS NWs have a strong dependence on the growth temperature. At low temperature, the ECS NWs are most likely in the form of Si/ECS core-shell structure. With the increase of growth temperature, the size of the Si core is reduced and finally disappeared. At high growth temperature, solid ECS NWs were obtained and longer PL lifetime and sharper XRD FWHM were observed, which indicates the improvements of crystal quality and optical properties.

The solid ECS NWs have longer PL lifetime at 1.5 μm than Si/ECS NWs. With the merits of high Er concentration and long PL lifetime, those ECS NWs can serve as optical gain material and have possible applications in amplifiers and lasers.

Chapter 4

CdS, CdSSe NWs

4.1 Growth of CdS NWs

In this part, pure CdS and CdSSe spatial composition graded single alloy NWs were synthesized by VLS method, their morphology and optical properties were studied. The first step of realizing the composition graded NWs is the controlled growth of CdS NWs. The control over the length of the NWs is very important for meeting different applications requirements.

A quartz boat with CdS powder was loaded at the center of the heating zone. Si wafers were sputtered with a 10 nm thickness Au film and placed at the downstream of the furnace. The furnace system was evacuated to a pressure below 0.2 Torr by mechanical pump. Then Nitrogen gas was introduced into the system and kept for 20 min to further eliminate oxygen in the tube. The system pressure can be controlled by a pressure controller valve, and NWs grown at different pressures from low pressure of 20, 40 Torr to high pressure of 140, 170, 200, and 225 Torr were obtained and the lengths of the NWs were compared. The NWs growths at different pressure were all optimized and repeated several times to verify the reproducibility of experimental results. And the growth time of all the experiments were 1.5 hours.

The morphology of the as grown samples was studied by SEM. Since the all the studied samples have uniform coverage of CdS NWs, the lengths data were randomly collected from 5 spots along the substrate. For those samples grown at

low pressure of 20, 40 Torr, the NWs typically have lengths ranging from 5—40 μm as shown in Figure 4.1 (a). At high pressure of 140—225 Torr, the typical wires lengths are in the range of 50—200 μm as shown in Figure 4.1 (b). The detailed comparison of the lengths of the CdS NWs is summarized in Table4.1 and Figure 4.2 gives the lengths distribution at different pressure.

(a) low pressure

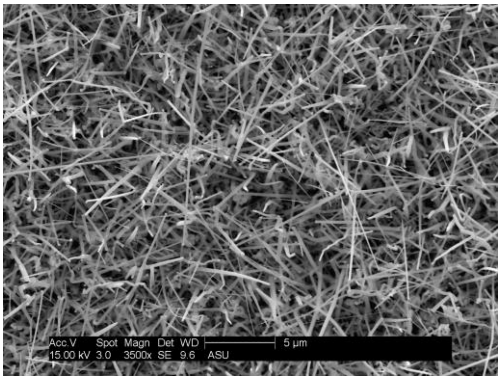

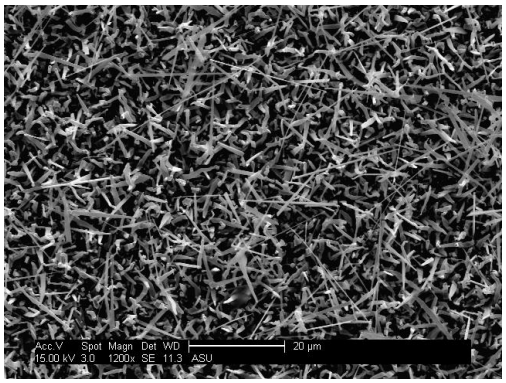

(b) high pressure

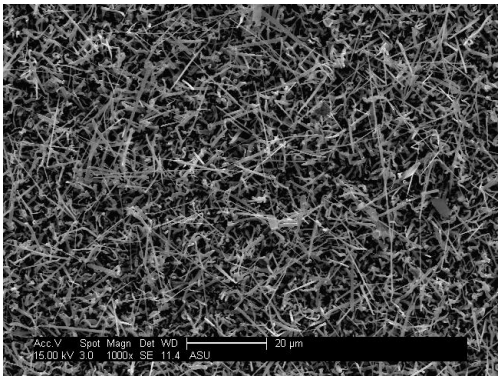

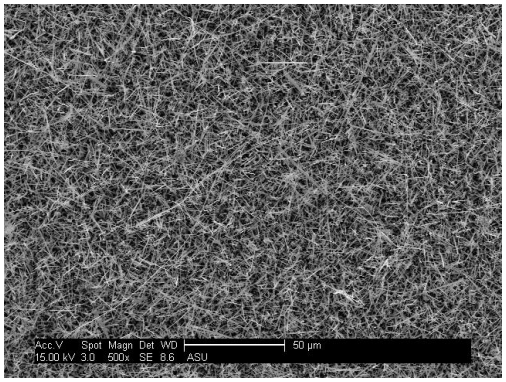

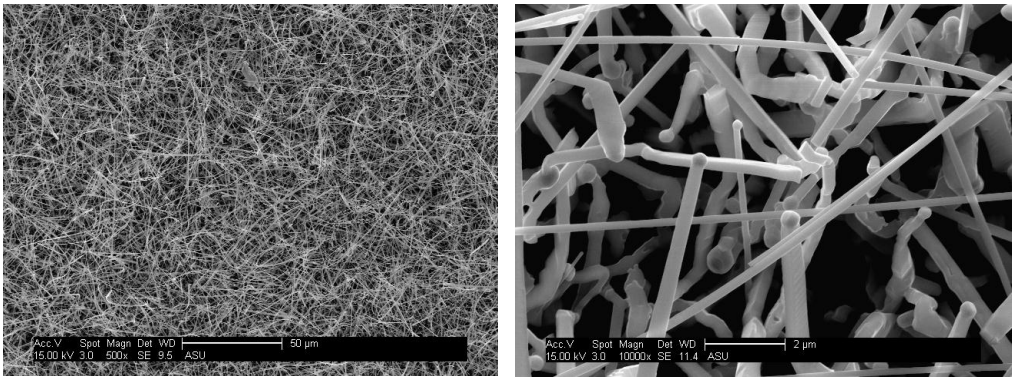

Figure 4.1 (a) CdS NWs grown at low pressure of 20 (left), 40 Torr (right) (b) high pressure of 140 (top left), 170 (top right), 225 (bottom left) Torr and zoomed in features (bottom right) of the NWs

Table 4.1 Comparison of the lengths of the NWs grown at different pressure

Pressure (Torr)	Length (μm)
20	5—20
40	20—40
140	50—80
170	60—150
225	100—200

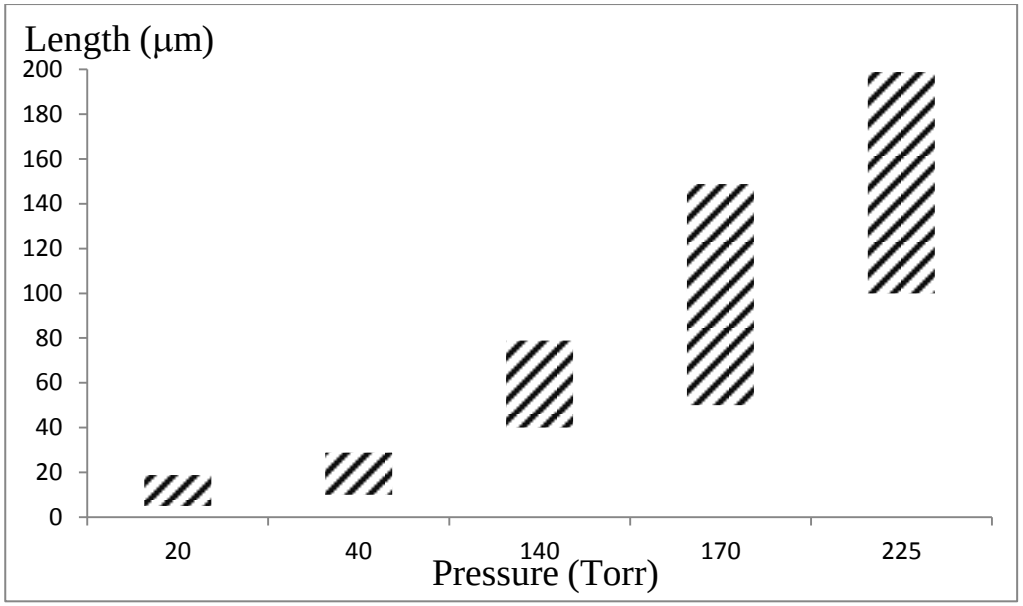

Figure 4.2 Comparison of lengths of CdS NWs/belts grown at different pressure of 20, 40, 140,170, 225 Torr, the dashed areas represent the lengths distribution

These results showed a clear trend that higher pressure produces longer NWs. This pressure—length relation provides another approach for the controlled growth of NWs. It enables better flexibility to grow NWs with different lengths to meet different application requirements and wires with longer length reduces the challenges for further manipulation and fabrication of the NWs.

4.2 Optical Properties of CdS NWs

PL experiments were performed to study the optical properties of the CdS NWs. CdS NWs were dispersed on the glass substrate first and then excited by Ti:sapphire laser pulses at the wavelength of 405 nm. Lasing measurement was carried out by exciting the NW using Nd:YAG laser at the third harmonics wavelength of 355 nm. The spectra were collected from one end of the NW. Figure 4.3 shows the PL and lasing spectra of single CdS NW. The linewidth of

the single CdS NW lasing peak is 0.8nm. Lasing observed in single CdS NW is also an indication of high crystal quality of the CdS NWs.

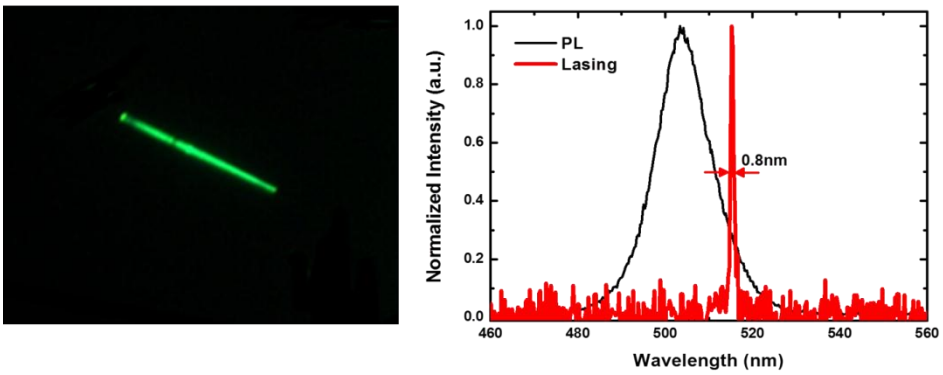

Figure 4.3 PL and lasing spectra of dispersed single CdS NW

4.3 Growth of CdSSe Composition Graded NWs

The strategy for realizing composition graded CdSSe are summarized by following steps:

(1) CdS section growth by only using the 3rd zone of the furnace.

(2) Adding CdSe part by turning on the heating elements in 1st and 2nd zone, meanwhile, decreasing the source temperature of CdS.

(3) Continue to grow CdSe rich part by keeping the entire furnace on.

The CdSSe NWs were obtained by following set-up. CdS powder was loaded at the 3rd zone of the furnace while CdSe powder was placed at the 1st zone of the furnace as shown in the Figure 4.4. There are ceramic wraps at the boundary of each heating zone to isolate each temperature regions. Si wafers sputtered with a 10 nm thickness Au film were used as substrates and placed at the downstream of the furnace. The CVD system was evacuate to a pressure below 0.2 Torr by

mechanical pump. Then 150 sccm Nitrogen flow was introduced into the system and kept for 30 min to eliminate oxygen in the tube and the system pressure was maintained at 225 Torr. Since the CVD furnace has 3 temperature zones, the source temperature, thus the source vapor concentration can be controlled readily in order to achieve different composition. The melting point of CdS powder is 1750 ℃ while CdSe powder is 1286 ℃. Thus, at same temperature, CdSe has lower evaporation rate compared to CdS. The 3rd zone was set at 900 ℃ and reached in 12 minutes. After 2 hours of CdS growth, the temperature of the 1st and 2nd zone are elevated to 850 ℃, meanwhile the 3rd zone temperature was decreased at a speed of 1 ℃/min. All the 3 zones reached 850 ℃ in 40 minutes. Finally, the furnace was kept at this temperature for 40 minutes for CdSe growth.

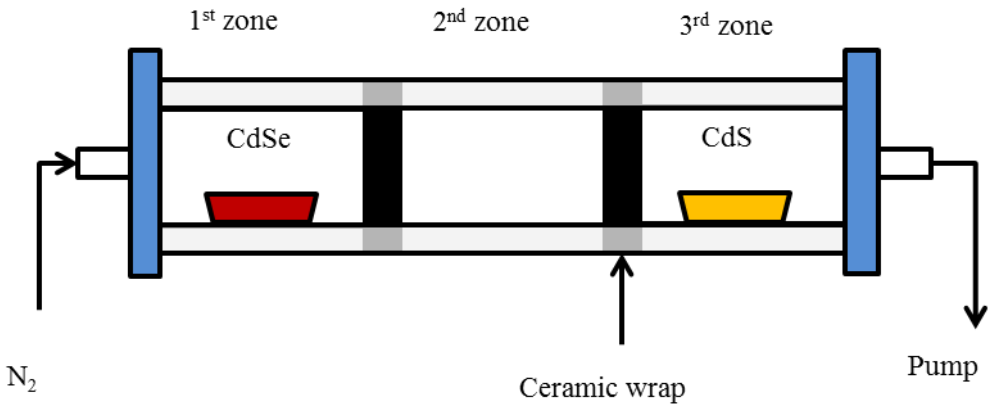

Figure 4.4 CdSSe composition graded NWs growth set-up

4.4 Optical Properties of CdSSe NWs

NWs were dispersed on the glass substrate and studied under laser illumination. The NWs typically have diameter of 200-500 nm and the length above 100 μm, the PL of the dispersed NWs are shown in Figure 4.5.

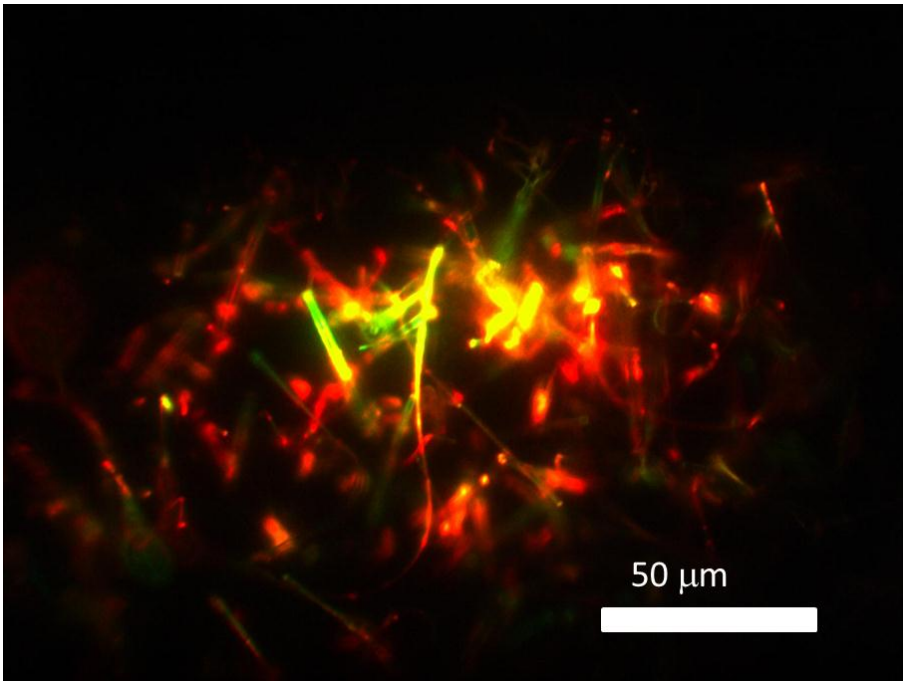

Figure 4.5 PL of dispersed CdSSe NWs

Figure 4.6 (a) shows the PL of a single CdSSe NW picked by a fiber tip. Then PL scan along the length of the NW was performed. Figure 4.6 (b) gives the emission from each spot scanned of the single wire, and the wavelength continuously tuned from 520 nm at one end to 620 nm at the other. These results indicate that the composition of the NW is tuning from CdS rich part to CdSe rich part corresponds to the 3 steps of the growth process.

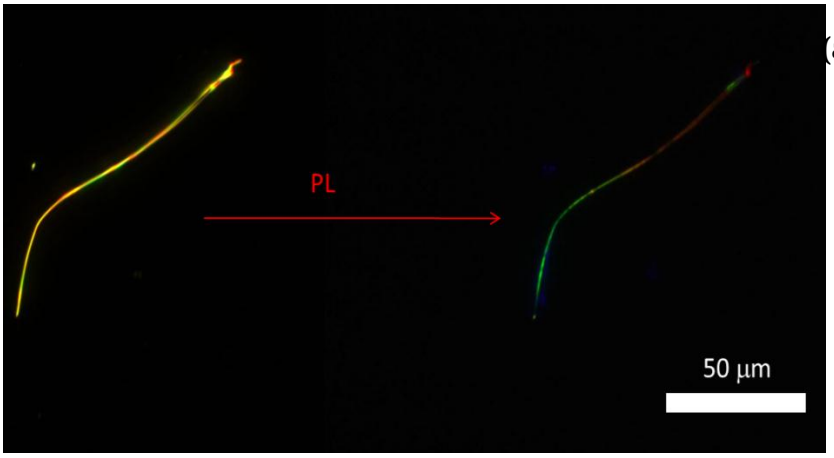

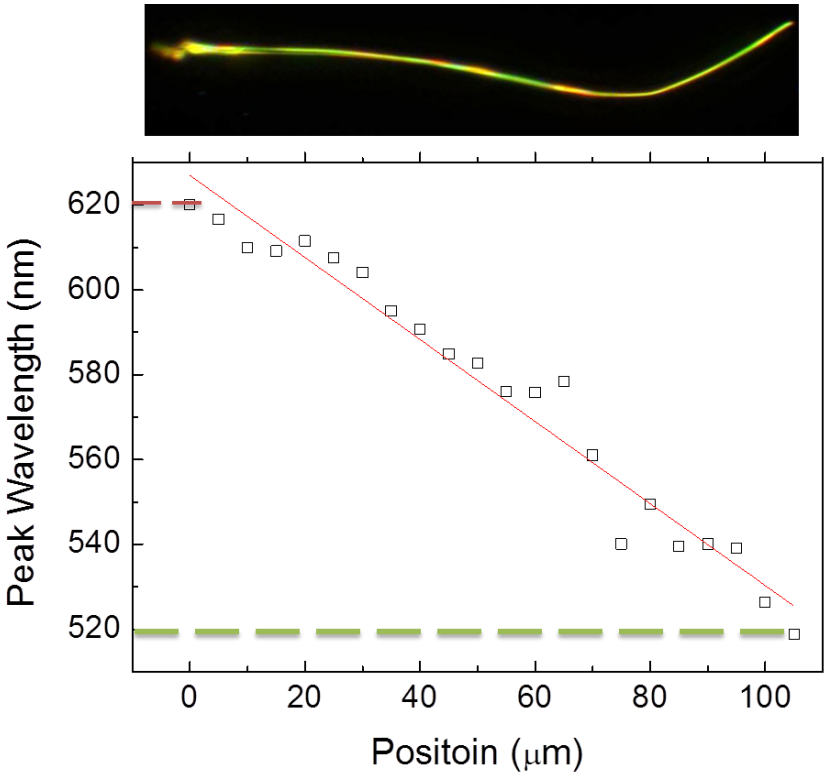

Figure 4.6 (a) PL image of single CdSSe NW (b) PL scan of the CdSSe single NWs

4.5 Growth Mechanism and Applications

The temperature control plays an important role for successful synthesizing composition grading along single CdSSe NWs. The composition of the VLS NWs growth is determined by the supplied vapor concentration of different source materials. At the beginning stage of the growth, only CdS source vapor was supplied to the substrate thus there was only CdS NW elongation. At the transition state of the growth, the CdSe source was heated up step by step, thus the concentration of CdSe increases correspondingly. Meanwhile, the source temperature of CdS was lowered, thus the concentration of CdS decreases. Also,

this is very important to maintain similar amount of material that was transported to the substrate. Otherwise, too much material supply may result in vapor-solid growth of big belts or sheets, as shown in Figure 4.7. For the entire growth process, the concentration of the vapor was tuning from CdS rich to CdSe rich, thus, the composition of the newly grown wires have composition tuning due to the change in the vapor concentrations.

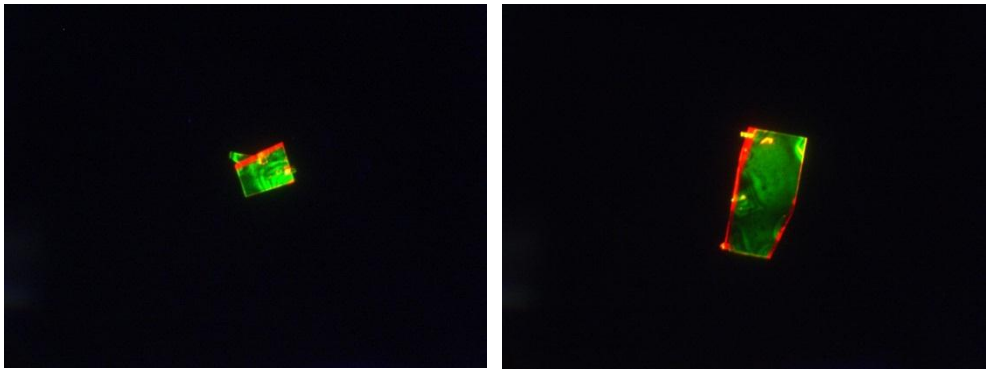

Figure 4.7 Dispersed nanoblet/nanosheet under PL illumination

These composition graded CdSSe NWs will have many very possible applications. For example, wavelength tunability and controllability are important for applications of a laser. Composition tuning in a single NW with diameter of a few hundred nanometer and controllable length provide another approach for realizing these functionalities. Moreover, since the CdSSe NWs have very wide wavelength coverage, it can be used as high efficiency solar cells. Also, with the inherent nature of large surface-to-volume ratio, NWs have higher photosensitivity than their bulk counterparts. Thus, composition graded can also be used as multispectral photodetectors. Another importance of these graded NWs is that multi-functionalities can be achieved in a single device, which largely simplifies the fabrication processes.

Chapter 5

Summary

1-D structures such as NWs have been recognized as one of the building blocks for future photonic devices due to their inherent unique properties. The success of the NWs based devices largely relies on the good understanding of their growth mechanism to have precise control over their parameters such as diameter, length, composition and so on. In this work, extensive NWs growth experiments and characterization were demonstrated.

In chapter 3, ECS NWs growths were systematically studied with an emphasis on growth temperature. It showed that with the increase of growth temperature, the NWs witnessed a transition from Si/ECS core-shell structure to solid ECS NWs with better crystal quality and optical properties. These ECS NWs have high Er concentration and long PL lifetime, thus, they have promising applications as optical gain material. In chapter 4, the strategy of synthesis CdS and CdSSe composition graded NWs were demonstrated. The lengths of the NWs have a strong correlation with the overall pressure. Growth at higher pressure typically produces NWs with longer length. The temperature control over source vapor concentration is the key to obtain the composition grading along single CdSSe NWs. These NWs have potential applications in multi-color light emission devices, photodetectors and solar cells.

REFERENCES

1 C. M. Lieber, Z. L. Wang, “Functional nanowires”, Mater. Res. Soc. Bull. **32**, 99-104 (2007)

2 B. Das, S. Subramanium, and M. R. Melloch, “Effects of electron-beam-induced damage on leakage currents in back-gated GaAs/AlGaAs devices”, Semicond.Sci.Technol. **8**, 1347 (1993)

3 R. A. Soref, “The past, present, and future of silicon photonics”, J. Sel. Top. Quantum Electron”, **12**, 1678-1687 (2006)

4 A. J. Kenyon, “Erbium in silicon”, Semicond. Sci. Technol. **20**, R65 (2005)

5 A. L. Pan, L. Yin, Z. Liu, M. Sun, P. L. Nichols, R. Liu, Y. Wang, and C. Z. Ning, “Single-crystal erbium chloride silicate nanowires as a Si-compatible light emission material in communication wavelengths”, Opt. Mater. Exp. **1**, 1202-1209 (2011)

6 R.Hill, “Energy-gap variations in semiconductor alloys”, J. Phys. C: Solid State Phys. **7**, 521 (1974)

7 M.H. Huang, Y. Wu, H. Feick, N. Tran, E. Weber, and P. Yang, “Catalytic growth of zinc oxide nanowires by vapor transport”, Adv. Mater. **13**, 113-116 (2001)

8 R. S. Wagner and W. C. Ellis, “The vapor-liquid-solid mechanism of crystal growth and its application to silicon”, Trans. Metall. Soc. AIME **233**, 1053-1064 (1965)

9 A. I. Hochbaum, R. Fan, R. He, and P. Yang, “Controlled growth of Si nanowire arrays for device integration”, Nano Lett. **5**, 457-460 (2005)

10 M.S. Gudiksen, J. Wang, and C.M. Lieber, “Synthetic control of the diameter and length of single crystal semiconductor nanowires”, J. Phys. Chem. B **105**, 4062-4064 (2001)

11 E. Ertekin, P. A.Greaney, D. C. Chrzan, and T. D. Sands, “Equilibrium limits of coherency in strained nanowire heterostructures”, J. Appl. Phys. **97** 114325-1-10 (2005)

12 Y. Li, F. Qian, J. Xiang and C.M. Lieber, Nanowire electronic and optoelectronic devices. Mater. Today **9** (10), 18-27 (2006)

13 Hugh O. Pierson, Handbook of Chemical Vapor Deposition, 2nd ed., Noyes Publications, 1999

14 Y. Cui and C.M. Lieber, "Functional Nanoscale Electronic Devices Assembled Using Silicon Nanowire Building Blocks", Science **291**, 851-853 (2001)

15 X. Duan, Y. Huang, Y. Cui, J. Wang, and C. M. Lieber, "Indium Phosphide Nanowires as Building Blocks for Nanoscale Electronic and Optoelectronic Devices", Nature, **409**, 66-69 (2001)

16 Y. Huang, X. Duan, C. M. Lieber., "Nanowires for Integrated Multicolor Nanophotonics", Small **1**, 142-147 (2005)

17 A. E. Siegman, Lasers, University Science Books, 1986

18 A.V. Maslov and C.Z. Ning, "Reflection of guided modes in a semiconductor nanowire laser", Appl. Phys. Lett. **83**, 1237-1239 (2003)

19 M. Zimmler, Jiming Bao, F. Capasso, S. Muller and C. Ronning, "Laser Action in Nanowires: Observation of the Transition from Amplified Spontaneous Emission to Laser Oscillation", App. Phys. Lett. **93**, 51101-51103 (2008)

20 M.H. Huang, S. Mao, H. Feick, H. Yan, Y. Wu, H. Kind, E. Weber, R. Russo, P. Yang, "Room-temperature ultraviolet nanowire nanolasers", Science **292**, 1897-1899 (2001)

21 J. A. Zapien, Y. Jiang, X. M. Meng, W. Chen, F. C. K. Au, Y. Lifshitz, and S. T. Lee, "Room-temperature single nanoribbon lasers". Appl. Phys. Lett. **84**, 1189-1191 (2004)

22 X. F. Duan, Y. Huang, R. Agarwal and C. M. Lieber, "Single-nanowire electrically driven lasers", Nature **421**, 241-245 (2003)

23 J. C. Johnson**,** H. J. Choi, K. P. Knutsen, R. D. Schaller, P. Yang, R. J. Saykally, "Single gallium nitride nanowire lasers", Nat. Mater. **1**, 106-110 (2002)

24 A.H. Chin, S. Vaddiraju, A.V. Maslov, C.Z. Ning, M.K. Sunkara and M. Meyyappan,. "Near-infrared semiconductor subwavelength-wire lasers",

Appl. Phys. Lett. **88**, 163115-163117 (2006)

25 S. Piscanec, M. Cantoro, A. C. Ferrari, J. A. Zapien, Y. Lifshitz, S. T. Lee, S. Hofmann, J. Robertson, "Raman spectroscopy of silicon nanowires", Phys. Rev. B **68**, 241312-241315 (2003)

26 M. Miritello, R. L. Savio, F. Iacona, G. Franzò, A. Irrera, A. M. Piro, C. Bongiorno, F. Priolo, "Efficient luminescence and energy transfer in erbium silicate thin films", Adv. Mater. **19**, 1582-1588 (2007)

27 R. Serna, M. Lohmeier, P. M. Zagwijn, E. Vlieg, and A. Polman, "Segregation and trapping of erbium during silicon molecular beam", Appl. Phys. Lett. **66**, 1385-1387 (1995)

28 H. Ennen, J. Schneider, G. Pomrenke, and A. Axmann, "1.54-μm luminescence of erbium-implanted III-V semiconductors and silicon", Appl. Phys. Lett. **43**, 943-945 (1983)

29 R. J. Mears, L. Reekie, I. M. Jauncey, and D. N. Payne, "Low Noise Erbium-Doped Fibre Amplifier Operating at 1.54 μm", Electron. Lett. **23**, 1026-1068 (1987)

30 C. P. Michael, H. B. Yuen, V. A. Sabnis, T. J. Johnson, R. Sewell, R. Smith, A. Jamora, A. Clark, S. Semans, P. B. Atanackovic, and O. Painter, "Growth, processing, and optical properties of epitaxial Er_2O_3 on silicon", Opt. Express **16**(24), 19649-19666 (2008)

31 H. Isshiki, M.J.A. de Dood, A. Polman and T. Kimura, "Self-assembled infrared-luminescent Er-Si-O crystallites on silicon", Appl. Phys. Lett. **85**, 4343-4345 (2004)

32 A. Polman, "Erbium implanted thin film photonic materials", J. Appl. Phys. **82**, 1-39 (1997)